Journal of Sound and Vibration, Volume 269, Issues 1-2, 6 January 2004, Pages 389-408.

Title:

MEASURING WAVE DYNAMICS IN I.C. ENGINE INTAKE SYSTEMS

Authors:

M.F. Harrison[*1] and P.T. Stanev [1]

[*]corresponding author

Professional addresses:

[1] School of Engineering, Cranfield University,
Cranfield, Bedfordshire MK43 0AL, England

Correspondence to:

Dr Matthew Harrison
School of Engineering
Whittle Building
Cranfield University
Cranfield
Bedfordshire MK43 0AL

Reference: MEASURING INTAKE WAVE DYNAMICS, Revision 1 (Final)
(14th November 2002)

Total number of pages: 27 of text (38 in total including this page)
Total number of figures: 16
5804 words

ABSTRACT

Wave dynamics in the intake system are known to strongly influence the performance of naturally aspirated internal combustion (I.C.) engines. Detailed measurements of the wave dynamics are required to: optimise the performance of an engine, to validate the results of an engine performance simulation or to better understand the physics of the intake system. Five different methods for making such measurements are discussed in this paper. Four are based on different forms of pressure measurement and one uses hot wire anemometry.

The different methods are investigated using results obtained on a single cylinder research engine. The different methods are used to produce measurements of fluctuating pressure and velocity as well as the specific acoustic impedance ratio of the intake pipe. Both time and frequency domain results are considered.

The paper concludes that no single method is perfect or indeed universally applicable to all situations and in a typical investigation of wave action more than one method is likely to be used. The combined use of two methods, wave decomposition and an unusual bi-directional pitot-static tube, seems to offer a robust reliable and useful strategy for measuring wave dynamics in the intake pipe that should prove successful on most IC engines.

1 Introduction

Wave dynamics in the intake system are known to strongly influence the performance of naturally aspirated internal combustion (I.C.) engines [1]. A suitably phased sound wave in the intake port can maintain a pressure ratio across the closing intake valve that remains favourable to inflow to the cylinder until the valve finally closes. The origin of such waves has been shown to be a resonant response of the intake duct to the forcing caused by the unsteady volume flow through the intake valve [2].

Detailed measurements of the wave dynamics are required to: optimise the performance of an engine, to validate the results of an engine performance simulation or to better understand the physics of the intake system. Five different methods for making such measurements are discussed in this paper. In choosing candidate methods for this study, all optical diagnostic techniques were precluded due to their need for optical access to the intake port. This decision was made in order that all methods considered might be suitable for all IC engines rather than being confined to special optical engines.

2 The test case

All measurements were made on a Ricardo E6 single cylinder engine. The 0.5 litre engine was fitted with a large airbox and orifice plate for airflow rate measurement. This was atop a 1.4m straight walled intake pipe as shown in Figure 1.

The intake system was equipped with a fixed venturi carburettor, although no fuel was delivered to this. Instead the engine was motored with the fuel and ignition systems

switched off. An earlier study [2] had shown that motored and firing wave dynamics were sufficiently similar to allow the sole study of the more convenient motored case. The effect of the airbox on the wave dynamics is also known to be small [3].

One end of the crankshaft is exposed on the Ricardo E6 and a slotted disk was attached to this. This was used along with an optical sensor to provide an instantaneous measure of crankshaft rotation with respect to the piston top dead centre position as well as an indication of engine speed.

The intake system was drilled and tapped at several locations along its length. Two Kistler type 4045A2 (2 bar) piezo-resistive pressure transducers were used on occasion as described in Section 3. These allow a direct measure of both static and dynamic pressures in the intake system. Their signals are amplified using two Kistler type 4611 amplifiers and the resulting fluctuating voltages were digitised using an Iotech Daqbook200 system and stored on a PC.

In-cylinder pressures were measured using a Kistler type 6117b (250 bar) measuring spark plug along with a Kistler type 5011 charge amplifier. The piezo-electric sensor does not give an indication of static pressure, only the fluctuating part so a particular calibration strategy was employed as described in Section 3.3 to overcome this.

The pressure drop across the orifice plate on the airbox was measured using a Druck type LP1500 (625 pa) differential pressure gauge.

In addition to these four pressure transducers a holder was fitted to the intake pipe to accommodate a single hot wire anemometer probe. The wire used was a Dantec type 55P11 that was 2.5μm thick and 2mm long. The holder ensured that the mean inlet flow was normal to the wire in order to preserve flow sensitivity [4].

Finally, a bi-directional pitot static probe was constructed. This was deliberately made to size so it could be screwed into any of the tappings made for the pressure transducers. This unusual probe is described in detail in Section 3.5.

The digitised signals recorded on the Iotech Daqbook200 system were post processed off line using codes written in Matlab™.

3 Experimental methods and results

Five experimental methods for the investigation of the intake wave dynamics were studied. The first is the conventional analysis of pressure records (Section 3.1). The second is a direct way of measuring the specific acoustic impedance spectrum (the ratio of fluctuating acoustic pressure to fluctuating particle velocity) at a position remote from the intake valve (Section 3.2). The third is an indirect way of measuring volume velocity time history through the intake valve (Section 3.3). The fourth and fifth are direct methods for measuring flow velocity time history using a hot wire anemometer (Section 3.4) and a bi-directional pitot static tube (Section 3.5) respectively.

3.1 Pressure time history analysis

Referring to Figure 1, one Kistler type 4045A2 pressure sensor was positioned in the wall of the 50mm diameter intake pipe, 550mm from the airbox. The engine was run and then motored at wide-open throttle and around 2000 rev/min^{-1}. Using the output of the optical crankshaft sensor, the pressure record from a single motored cycle is shown against one from the running (firing) engine in Figure 2. The physics of the intake process that cause such intake pressure records is discussed elsewhere [2]. The intention here is to discuss the practicalities of this method and the usefulness of the results.

Figure 2 shows a pressure time history along with an average spectrum of the motored pressure record. The latter is obtained by performing a 2048 point FFT on a signal acquired at 4096Hz, thus producing a spectrum with 2Hz resolution. A moving Hanning window with variable length overlap allows many such FFTs to be generated from a modest length data sequence and a reliable average spectrum is therefore obtained.

The usefulness of the single pressure record is greatly enhanced if a crankshaft sensor enables the labelling of the record with key events (intake valve opening (IVO), exhaust valve closing (EVC), 90^{o} after top dead centre (ATDC), bottom dead centre (BDC) and intake valve closed (IVC)). A well-behaved engine that is firing, will be without sudden pressure gradient reversals at around IVO, EVC or IVC that signify

outflow from the cylinder and will also exhibit a high-pressure peak 20-50^o before IVC [2].

In the case shown in Figure 2 the crankshaft sensor could not be used directly to label the pressure record as the pressure was measured some 850mm from the intake valve and the propagation delay from the valve to this position was unknown. The propagation delay can be estimated by assuming that the propagation of pressure from the valve occurs at a speed given by the speed of sound minus the spatial average flow velocity. Assuming 343ms^{-1} for the former and 15ms^{-1} for the latter, for the case shown in Figure 2, the position of labels IVO, EVC etc would have to be retarded by 29.4^o to correct for the time of flight between the intake valve and the pressure sensor.

There are two alternatives to this method for correcting the IVO, EVC etc labels. The expensive alternative is to position a second pressure sensor near the valve and plot that with its correct labels. Assuming that the pressure wave does not distort as it propagates, the data from the remote position can be shifted so that it lines up with the data recorded at the valve. The cheaper alternative to this is to briefly interrupt the ignition (for a spark ignition engine) or the fuel injection (for a common rail diesel engine), which often results in a flow reversal between IVO and EVC, which can be used as a timing mark. This particular technique has been used for Figure 2.

The plotting of a pressure spectrum along with the pressure record gives insight into the wave dynamics. The dynamics are those of a resonant system, exited by the unsteady flow through the valves [2]. The lowest frequency peak in the spectrum (at frequency f_0) yields an estimate of the engine speed:

$$\text{Engine speed} = f_o \times 120 \text{ rev/min}^{-1} \quad (1)$$

which is 1980 rev/min in the case of Figure 2, and the frequency of dominant peak (at frequency f_1) yields an estimate of the acoustic length, x, of the intake pipe.

$$x = \frac{343}{4 f_1} (\text{m}) \quad (2)$$

which is 1.34m in the case of Figure 2.

3.2 Wave decomposition

Consider a pressure wave originating at the opening intake valve and propagating towards the open end of the intake duct where it is strongly reflected. Due to the cyclic operation of the I.C. engine such waves are created continuously and they interact to form a complex distributed sound field in the intake system. That sound field may be described in space and time using positive and negative (with reference to positive spatial coordinate x) travelling wave components p^+ and p^- respectively.

$$P(x,t) = p^+ e^{i(\omega t - kx)} + p^- e^{i(\omega t - kx)} \quad (3)$$

where P (x, t) is the fluctuating acoustic pressure at frequency ω rads^{-1} and k is the wavenumber.

Equation (3) can be re-written in terms of frequency and the spatial coordinate, thus:

$$P(\omega, x) = p^{+} e^{-ikx} + p^{-} e^{ikx} \qquad (4)$$

If pressure spectra are found at two locations in the intake pipe that are close together (50-150mm apart) then a pair of simultaneous equations is constructed, each in the form of equation (4) and these can be solved algebraically to obtain p^{+} and p^{-}. This is the basis of the now well-understood wave decomposition method [5-7]. In the work reported here, a particular variant of the method is used [8].

Referring to Figure 1, one Kistler type 4045A2 piezo-resistive pressure sensor is positioned at a distance x_1 = 550mm from the airbox and another at x_2 = 700mm from the airbox. Their amplified signals are recorded directly onto a HHB type MDP500 mini-disc recorder, which has the effect of AC coupling the signals, thus, isolating the fluctuating pressure from the total pressure sensed by the pressure sensor

A comment is needed on the implications of using the mini-disc recording system for these measurements. The MDP500 recorder was first considered for use because it offered an inexpensive way of recording a pair of long pressure time histories with high signal to noise ratio. It is well known that the mini-disc recording system employs a particular form of data compression that normally makes it unsuitable for laboratory grade measurements. As it was not possible to pre-judge the effects of the data compression on the results obtained from wave-decomposition, a validation exercise was undertaken before the MDP500 was accepted for use [8]. Wave-decomposition measurements were made in a length of straight pipe, strongly excited with broadband white noise, and in the absence of mean flow. The acoustic reflection

coefficient at the open end of the tube was measured and found to agree well with linear acoustic theory [9] in the frequency range of interest (20-2000 Hz). Notwithstanding concerns over the effects of data compression, the MDP500 was accepted for use in the particular case of wave-decomposition on the basis that no evidence of corruption was found in the results of the validation exercise.

We can write:

$$P_1(\omega_1 x_1) = p^+ e^{-\beta^+ x_1} + p^- e^{i\beta^- x_1} \tag{5}$$

$$P_2(\omega_1 x_2) = p^+ e^{-\beta^+ x_2} + p^- e^{i\beta^- x_2} \tag{6}$$

where $$\beta^+ = \frac{k + \alpha(1-i)}{1+M} \tag{7}$$

and $$\beta^- = \frac{k + \alpha(1-i)}{1-M} \tag{8}$$

are complex wavenumbers that take account of the effects of visco thermal attenuation through the attenuation coefficient α and mean flow speed through the Mach number M [9]. The attenuation coefficient is given by [9]

$$\alpha = \frac{1}{ac_0}\left[\frac{\nu\omega}{2}\right]^{0.5}\left[1+(\gamma-1)P_r^{-0.5}\right] \tag{9}$$

γ = ratio of specific heats

a = pipe radius (m)

c_o = stagnation speed of sound (ms^{-1})

P_r = Prandtl number

ν = kinematic viscosity

Equations (5) and (6) can be re-written:

$$E_{11} = p^+ K_1 + p^- K_2 \tag{10}$$

$$E_{22} = p^+ K_3 + p^- K_4 \tag{11}$$

where E_{11} and E_{22} are autospectra of P_1 and P_2 respectively.

The simultaneous pair (10) and (11) could be solved algebraically for p^+ and p^- if two perfectly identical phase-matched pressure sensors were used. For a pair of practical sensors, some cross calibration is required.

With the pressure sensors at positions x = 0.55m and 0.70m respectively, a matrix $\mathbf{S_P}$ of auto and cross spectra can be formed:

$$\mathbf{S_P} = \begin{bmatrix} E_{11} & E_{12} \\ E_{21} & E_{22} \end{bmatrix} \tag{12}$$

This should be recorded at every engine speed of interest. For this study a 25-second sample of data was recorded and then digitised using the Iotech Daqbook200 at a

sample rate of 8192Hz. 1024 point FFTs were used with a moving Hanning window and variable overlap (15% chosen) to produce the matrix $\mathbf{S_P}$ based on the average of 100 FFT calculations for each signal with a frequency resolution of 8Hz.

Referring to Figure 1, if the lower pressure sensor is moved so that it is located in the same x-plane as the other sensor a new matrix of auto and cross spectra, **F**, can be found for each engine speed of interest.

$$\mathbf{F} = \begin{bmatrix} E_{11} & E_{12} \\ E_{21} & E_{22} \end{bmatrix} \tag{13}$$

It is important to use the same sampling frequency and the same FFT length as used for $\mathbf{S_P}$. When that is the case we can form the correction matrix **G**.

$$\mathbf{G} = \mathbf{F}. / \mathbf{F}(1,1) \tag{14}$$

An amplitude and phase corrected version of $\mathbf{S_P}$ is:

$$\mathbf{S_P^*} = \frac{\mathbf{S_P}}{\mathbf{G}} \tag{15}$$

As both pressure sensors are located in the same x-plane when **F** is generated, they should be exposed to the same instantaneous values of pressure if the mean flow is steady and the frequency of sound is less than the planar cutoff frequency (3580Hz in this case). In other words, the two pressure signals should be perfectly correlated in **F**. The coherence between the two signals in **F** is near unity below 1100Hz when the

engine is motored at 2000 rev/min (as shown in Figure 3) and, therefore, the degree of correlation is high at low frequency but poor at higher frequencies. Inspection of the pressure spectrum in Figure 2 shows low levels of excitation at frequencies above a few harmonics of the cycle frequency, therefore, poor signal to noise and, hence, poor coherence is expected at higher frequencies.

Figure 4 shows the coherence σ applicable to $\mathbf{S}_\mathbf{P}^*$

$$\sigma = \frac{\left[\mathbf{S}_\mathbf{P}^*(1,2)\right]^2}{\mathbf{S}_\mathbf{P}^*(1,1).\mathbf{S}_\mathbf{P}^*(2,2)} \tag{16}$$

The compound effect of two sets of limited signal to noise ratio $\mathbf{S}_\mathbf{P}^*$ (first in $\mathbf{S_P}$ and then in **G**) is shown in reduced coherence at all frequencies above 200Hz.

Returning to the wave decomposition itself we can re-write (10,11) as:

$$\mathbf{S}_\mathbf{P}^*(1,1) = p_1^+ K_1 + p_1^- K_2 \tag{17}$$

$$\mathbf{S}_\mathbf{P}^*(1,2) = p_1^+ K_3 + p_1^- K_4 \tag{18}$$

and solve these algebraically to yield:

$$p^+ = \frac{\mathbf{S}_\mathbf{P}^*(1,1) - \left[\mathbf{S}_\mathbf{P}^*(1,2).\left(\frac{K_2}{K_4}\right)\right]}{K_1 - \left[K_3\left(\frac{K_2}{K_4}\right)\right]} \tag{19}$$

$$p^{-} = \frac{\mathbf{S}_{\mathbf{P}}^{*}(1,1) - p^{+} K_1}{K_2} \tag{20}$$

p^+ and p^- are complex values of the wave component amplitude at a plane in the duct. If in equations (5,6) $x_1 = 0.45$m and $x_2 = 0.3$m the p^+ and p^- are calculated for a plane that is 1m from the airbox. The reflection coefficient at that plane is given by:

$$r = \frac{p^{-}}{p^{+}} \tag{21}$$

and the real and imaginary parts of this are shown in Figure 5,6 respectively. A calculation of the real and imaginary parts, based on linear plane-wave acoustic theory [2] is also shown. The agreement between theory and experiment is good as long as the coherence of the measured pressure signals remains high (Figure 4).

The specific acoustic impedance ratio ζ is given by:

$$\zeta = \frac{1+r}{1-r} = \frac{1}{\rho_0 c_0}\left[\frac{P}{u}\right] = \frac{1}{\rho_0 c_0}\left[\frac{PS}{U}\right] \tag{22}$$

ρ_o = stagnation density (kgm^{-3})

u = particle velocity (ms^{-1})

U= volume velocity ($m^3\ s^{-1}$)

S = cross sectional area of the intake pipe

and measured results are plotted alongside theoretical calculations for the case of 2000 revmin^{-1} in Figure 7. The agreement is good at frequencies below 200Hz where the coherence is high (Figure 4).

So the wave decomposition technique allows the direct measurement of acoustic impedance at a plane in the intake duct. The first use for this is in the assessment of resonant frequencies (where ζ goes to a maximum) although for this the reference plane should be the intake valve and one of the pressure sensors should be placed nearby which is not always easy.

A second use is in the refinement of engine simulation models. These involve the time domain solution of the gas dynamics in the intake system. Appropriate acoustic end corrections are added to some pipe lengths in order that the computed results may match measured results [10]. These end corrections can be found by experiment using the wave decomposition method.

$$r = R\, e^{i\theta} = -R\, e^{i2kl_m} \tag{23}$$

where l_m is the physical length plus the end correction.

3.3 Pressure drop across the intake valve

The unsteady mass flow through the intake valve (in kgs^{-1}) is routinely calculated using the well-known model [10].

$$\dot{m} = \frac{P_C A_e}{c_C}\left[\left(\frac{2\gamma^2}{\gamma-1}\right)\left(\frac{P_1}{P_C}\right)^{2/\gamma}\left[1-\left(\frac{P_1}{P_C}\right)^{\frac{\gamma-1}{\gamma}}\right]\right]^{1/2} \quad (24)$$

where

P_C = cylinder pressure (Pa)

P_1 = intake port pressure (Pa)

c_c = speed of sound in the cylinder

$A_e = A_m C$

A_m = valve open area (m^2)

C = flow loss coefficient (measured on a flow bench)

This will normally be part of an engine simulation where P_C and P_1 are also calculated. However, if P_C and P_1 are in fact measured quantities then the unsteady mass flow through the valve may valve may be measured indirectly [11].

To make this measurement, the open area under the intake valve must be known throughout the engine cycle and an appropriate set of empirical flow loss coefficients measured or selected. In this case, these were already well defined for the Ricardo E6 engine.

A Kistler type 4045A2 piezo-resistive pressure transducer was located in the intake port, close to the intake valve. A piezo-electric pressure transducer (Kistler type 6117b) replaced the regular spark plug used with the engine. The engine was motored at various speeds and signals from the sensors were digitised using the Iotech Daqbook200 system along with the output from the optical crankshaft sensor.

As already mentioned, the Kistler type 6117b pressure sensor does not measure static pressures and, hence, (even when the engine is motored to avoid thermal shock to the sensor) there is some uncertainty over the absolute calibration of the output signal. A common technique to limit the effect of this is to use a piezo-resistive pressure sensor in the intake port and to DC shift the pressure data obtained from the piezo-electric device so that it matches that from the piezo-resistive device when the piston is at the bottom dead centre of the intake stroke.

A refinement of that technique has been applied here. Having done that, measured and DC shifted data for P_C is used along with measured data for P_1 in Equation 24 to calculate the unsteady mass flow during the intake period (IVO – IVC). The time integral of that mass flow rate time history is then compared to the mass flow rate measured using the orifice plate fitted to the airbox (Figure: 1). The DC shift applied to the cylinder pressure (some 2-3 bar) is then adjusted until the two measures of mass flow rate agree. For the case of 1921 rev/min the corrected cylinder pressure is shown against the measured port pressure in Figure 8. The resulting air mass flow rate is shown in Figure 9. The flow reversal soon after IVO (as predicted in Figure 2) is shown as a negative mass flow rate denoting outflow from the cylinder.

The corrected cylinder pressure in Figure 8 is actually the ensemble average of the data from 10 cycles. The equally spaced dips in the data are due to electro-magnetic noise that frequently corrupt signals obtained using such sensors [12]. If this were removed by filtration the trace in Figure 9 would be much smoother.

If we make the simplifying assumption that the density of the intake flow remains at the stagnation density (1.19 kg m^{-3} in this case) then we can calculate the volume velocity through the valve. Knowing the instantaneous open area under the valve we can easily calculate the flow velocity through the valve as shown in Figure 10. The flow reversal has a velocity that is instantaneously sonic shortly after IVO but the average flow speed through the valve is more like 0.25M.

The calculated volume velocity also allows the calculation of the flow velocity in the narrow intake port (Figure 11 : 0.15M typical) and in the wider intake pipe (Figure 12 : 0.07M typical).

This method is a useful way of measuring the volume velocity source strength of the intake process which is the cause of the wave action in the intake pipe [2]. The results can be compared directly with those computed by engine simulation for an alternative form of validation of the calculated results. For engine developers, the method also quantifies the extent of any flow reversals soon after IVO that will reduce volumetric efficiency.

3.4 Hot wire anemometry

A single wire constant temperature anemometer can be used to measure the amplitude (but not the direction) of the flow at one point in the intake system. The electronics of the system contains a Wheatstone bridge circuit with the sensor as one arm of the bridge, and two fixed values resistors and one variable resistor completes the circuit [13]. A differential feedback amplifier senses the bridge unbalance and adds current

to hold the sensor temperature (and, hence, resistance) constant when the wire is being cooled by a gas flow. The voltage across the bridge is proportional to the gas velocity and the sensitivity of the sensor is governed by the wire temperature.

The Wheatstone bridge is only balanced at one velocity and becomes unbalanced as the velocity changes. The feedback amplifier is fast acting giving a nearly balanced circuit a good high frequency response. The frequency response of the circuit may be tested using a square electrical wave input and a dummy electric resistor in place of the hot wire [13]. A high frequency response will allow the square wave to be reproduced faithfully.

The frequency response of the actual probe in the circuit must be checked in a fluid at the same velocity to be measured. The bandwidth of the sensor and signal conditioning can then be maximised by tuning the settings of the electronics. This proved difficult in this case as the flow velocity in the intake pipe varies strongly even through one four-stroke cycle but with perseverance a compromise setting was found that gave adequate sensitivity and acceptable bandwidth.

The balancing of the Wheatstone bridge and the subsequent calibration of the system were performed using the experimental set-up shown in Figure 13. Compressed air passes through a filter and then a regulating valve and into a calibration unit where it emerges as a free jet. A differential pressure manometer measures the pressure drop across the nozzle and the free stream flow velocity *v* is calculated from:

$$v = \sqrt{\frac{2 \Delta P_{NOZZLE} R T_{amb}}{P_{amb}}} \qquad (25)$$

where P_{amb} and T_{amb} are ambient pressure and temperature respectively, R is the universal gas constant and ΔP_{NOZZLE} is the pressure difference measured across the nozzle.

The hot-wire is exposed to a flow having a known velocity and a voltage output from the signal conditioning is measured. This is repeated for varying flow velocities. Flow speed is controlled by changing the nozzle size and by using the air supply control valve.

For flow speeds up to 15m/s a fourth order polynomial was used to describe the relationship between flow speed and the voltage recorded during the calibration. At higher speeds the calibration is based on a linear law. This composite calibration was used when experimenting on the engine intake along with a Butterworth low pass filter set at 64Hz (the dominant frequency of oscillation in the intake pipe – Figure 2). This was needed to overcome severe problems with electromagnetic noise on the hot-wire signals. This was found to be an unavoidable output from the dynamometer.

It should be noted that the hot wire anemometer system cannot be used to measure velocities downstream of the carburettor, with a firing engine, as the evaporating fuel droplets would affect the calibration of the device.

The results of the hot-wire experiment at around 2000 rev/min is shown in Figure 14. The calibrated output of the hot-wire signal is of course a rectified oscillation and the forward-reverse flow ambiguity is overcome by declaring that negative flow velocity

is accompanied by a pressure depression. This also makes the comparison of pressure and velocity records easier on the eye.

The magnitude of the velocity in the period IVO-IVC agrees well with that found from an indirect measurement of the flow through the intake pipe (Section 3.3) Figure 12.

After IVC there is only a small mean flow in the intake pipe and the velocity recorded is that of a rapidly decaying oscillation about decaying mean flow velocity.

One should note that the fluctuating pressure and velocities are not measured in the same axial position. The pressure measurement was made some 0.15m upstream of the hot wire so that the pressure sensor did not foul the hot wire probe. Also the second plot in Figure 14 shows the fluctuating torque recorded during the experiments.

3.5 Bi-directional pitot static probe

A rather unusual bi-directional pitot static probe was trialled. This was a development of a much less sensitive earlier device [15]. The layout of the device is shown in Figure 15. The device uses two Kistler Type 4045A2 piezo-resistive pressure transducers located in the same plane of the intake pipe. The first measures the static pressure. The second measures a pressure quantity that approximates to the total pressure.

This second sensor is fitted to a probe. The probe has two narrow bore pipes protruding from a small chamber directly in front of the pressure sensors. The tubes are bent so that one faces directly into the inflow in the pipe, and the second faces directly into the reverse flow.

The difference between the voltage signals from the two pressure sensors is an approximation of the fluctuating dynamic head resolved into two flow directions.

With the engine motored at 2000 rev/min a dynamic calibration has been achieved by comparing the largest voltage difference obtained from the two sensors with the largest flow velocity measured with a hot wire (Figure 14).

Figure 16 shows a measurement of the oscillating flow velocity in the intake pipe obtained using the bi-directional pitot-static probe calibrated with respect to hot wire results obtained earlier.

The device seems to have adequate frequency response. It is interesting to note that the rate of decay of the oscillating velocity after IVC is less in these results than those obtained using the hot wire. The decay rate obtained for the velocity using the bi-directional pitot static probe matches the decay rate seen in the corresponding pressure records whilst the same is not true for the hot wire anemometer results. This is probably due to the effects on the hot wire results of using a combination of fourth order polynomial and linear laws to describe the calibration across a wide variation in velocity.

4 Discussion

Five experimental methods of measuring wave action in the intake system of an IC engine have been investigated. No single method is perfect or indeed universally applicable to all situations and in a typical investigation of wave action more than one method is likely to be used.

The main strengths and weaknesses of each method are as follows:

1. Pressure time history analysis; Strengths – simple and robust; Weaknesses – only provides information on pressure fluctuations and not on the accompanying velocity fluctuations.

2. Wave decomposition; Strengths – measures the specific acoustic impedance ratio directly; Weaknesses – only reliable at low frequencies, only provides the ratio of pressure and velocity, cannot distinguish between the open valve and closed valve cases.

3. Pressure drop across the intake valve; Strengths – provides pressure and velocity time histories; Weaknesses – only works for the portion of the engine cycle when the intake valve is open, prone to the ill effects of noisy pressure signals, needs a large quantity of empirical data relating to the engine (flow loss coefficients, valve lift curves and intake port and valve dimensions) to calculate the final results.

4. Hot wire anemometry with pressure measurements; Strengths – gives pressure and velocity time histories for the whole engine cycle; Weaknesses – cannot be used when fuel is introduced to the intake flow, fragile wires have a limited service life, calibration is difficult to perfect.

5. Bi-directional pitot-static tube; Strengths – robust with good dynamic and frequency response; Weaknesses – requires calibration against another method of velocity measurement such as a hot wire anemometry

Inspecting the strengths and weaknesses of the alternative methods it seems that using wave decomposition to measure the effective acoustic length of the intake pipe (actually the specific impedance ratio is measured and the effective length is determined using an acoustic model and reverse engineering) and using the bi-directional pitot static probe to measure oscillating pressure and velocity time histories seems to be a generally applicable and useful measurement strategy.

5 Conclusions

Of the five methods investigated, the combined use of wave decomposition and the bi-directional pitot-static tube seems to offer a robust, reliable and useful strategy for measuring wave dynamics in the intake pipe that should prove successful on most IC engines.

Acknowledgements

The authors gratefully acknowledge the support of EPSRC under Grant No: GR/R04324 for this work.

References

1 A. Ohata, Y. Ishida, 1982, SAE Paper No. 820407, Dynamic inlet pressure and volumetric efficiency of four cycle four cylinder engine.

2 M. F. Harrison and P. T. Stanev, 2002, Provisionally accepted for publication by the Journal of Sound and Vibration, A linear acoustic model of intake wave dynamics in I.C. engines.

3 S. Gritsis, 2001, MSc Thesis: Cranfield University, Internal combustion engine intake acoustics

4 T. H. Dracos (Editor), 1996, Kluwer Academic Publishers, Three-dimensional velocity and vorticity measuring and image analysis techniques – lecture notes from the short course held in Zurich, Switzerland, 3-6 September 1996.

5 P. O. A. L. Davies, J. L. Bento Coelho, M. Bhattacharya, 1980, J. Sound Vib. 72(4), 539-542, Measurement of plane wave acoustic fields in flow ducts.

6 K. R. Holland, P. O. A. L. Davies, 2000, J. Sound Vib., 230(4), pp915-932, The measurement of sound power flux in flow ducts,

7 P. O. A. L. Davies, K. R. Holland, D. van der Walt, 1999, 5682/004/99, Sound power flux measurements in exhaust systems, Published in “Noise and Vibration – Advances in Research and Development”, IMechE Seminar Publication, 2000

8 P. L. Rubio Unzueta, 2001, MSc Thesis: Cranfield University, Quantifying throttle losses.

9 P. O. A. L. Davies, 1988, J. Sound Vib., 124(1), pp91-115, Practical flow duct acoustics.

10 D. E. Winterbone, R. J. Pearson, 1999, Professional Engineering Publishing, Design techniques for engine manifolds – wave action methods for IC engines.

11 A. Dunkley, 2000, MSc Thesis: Cranfield University, The acoustics of IC engine manifolds.

12 M. Plint, A. Martyr, 1999, Butterworth-Heinemann, Engine testing – theory and practice (2^{nd} edition).

13 C. G. Lomas, 1986, Cambridge University Press, Fundamentals of hot wire anemometry.

14 W. K. George, P. D. Beuther, M. Ahmad, 1981, Experimental Thermal and Fluid Science, 2, 230-235, Polynomial calibrations for hot wires in thermally varying flows.

15 W. R. Brandsteter, M. J. Car, 1973, SAE Paper No. 73/0494, Measurements of air distribution in a multi-cylinder engine by means of a mass flow probe.

Figure captions

Figure: 1 Single cylinder test engine.

Figure: 2 Average spectrum of a long pressure time history. Motored 1891 revmin^{-1}(solid line), firing 1866 revmin^{-1} (dashed line).

Figure: 3 Calibration in the wave decomposition method: coherence between two pressure records in the same plane of the intake pipe, at 2000 revmin^{-1}.

Figure: 4 The wave decomposition method: coherence between two cross-calibrated pressure records in different planes of the intake pipe, at 2000 revmin^{-1}.

Figure: 5 Real part of the reflection coefficient in a plane of the intake duct. Measured (solid line) and calculated (dashed line) at 2000 revmin^{-1}.

Figure: 6 Imaginary part of the reflection coefficient in a plane of the intake duct. Measured (solid line) and calculated (dashed line) at 2000 revmin^{-1}.

Figure: 7 Specific acoustic impedance ratio in a plane of the intake duct. Measured (solid line) and calculated (dashed line) at 2000 revmin^{-1}.

Figure: 8 Pressures either side of the intake valve. Measured at 1921 revmin^{-1}.

Figure: 9 Mass air flow rate through the intake valve. Measured at 1921 revmin^{-1}. Cylinder pressure (solid line) intake port pressure (dashed line).

Figure: 10 Volumetric air flow rate through the intake valve. Measured at 1921 revmin^{-1}.

Figure: 11 Air flow velocity through the intake port. Calculated from a measurement at 1921 revmin^{-1}.

Figure: 12 Air flow velocity through the intake pipe. Calculated from a measurement at 1921 revmin^{-1}.

Figure: 13 Hot wire-anemometer calibration. 1 Air supply, 2 Filter, 3 Pressure valve, 4 Hot-wire calibration unit, 5 Differential pressure transducer, 6 Hot-wire, support and traverse mechanism, 7 Weatstone and feedback amplifier, 8 Voltmeter, 9 Oscilloscope, 10 Digital data acquisition,

Figure: 14 Signal from top dead centre indicator, engine torque, pressure in the intake pipe, air flow velocity through the intake pipe measured at 1891 revmin^{-1}using hot wire anemometer.

Figure: 15 Bi-directional pitot-static tube measurement system.

Figure: 16 Signal from top dead centre indicator, pressure in the intake pipe, air flow velocity through the intake pipe measured at 1891 revmin^{-1}using bi-directional pitot static tube.

Figures

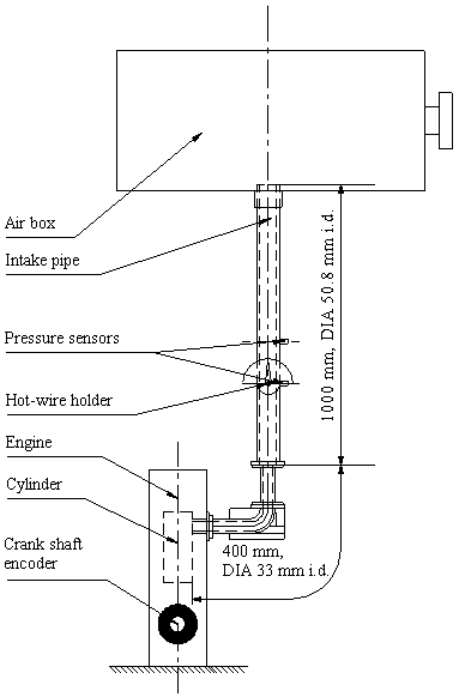

Figure: 1

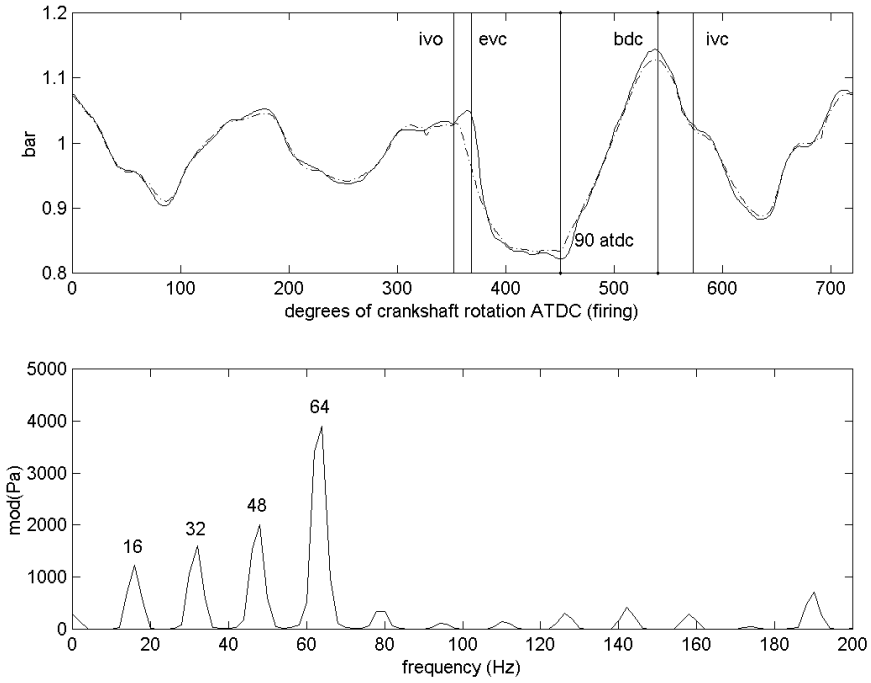

Figure: 2

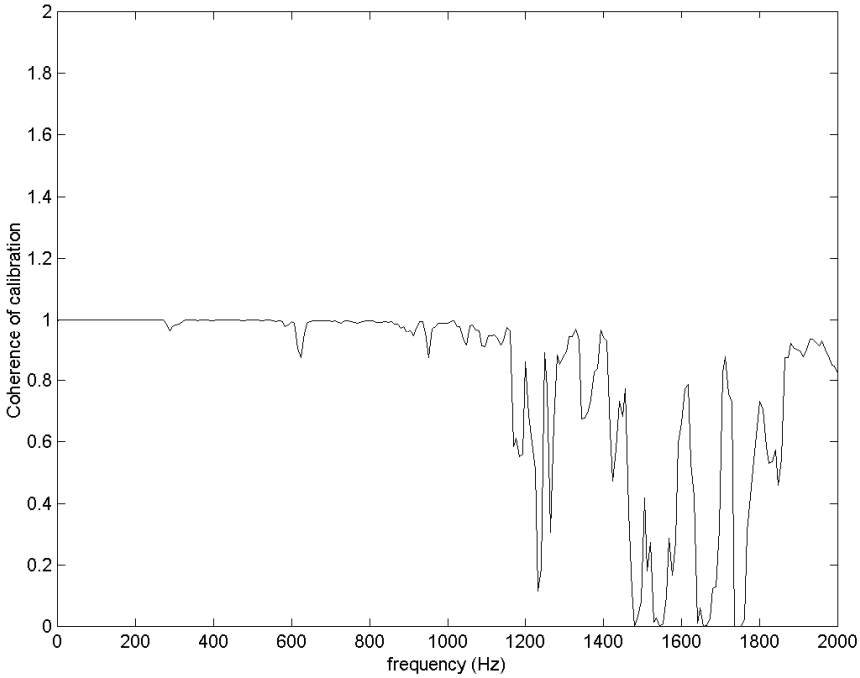

Figure: 3

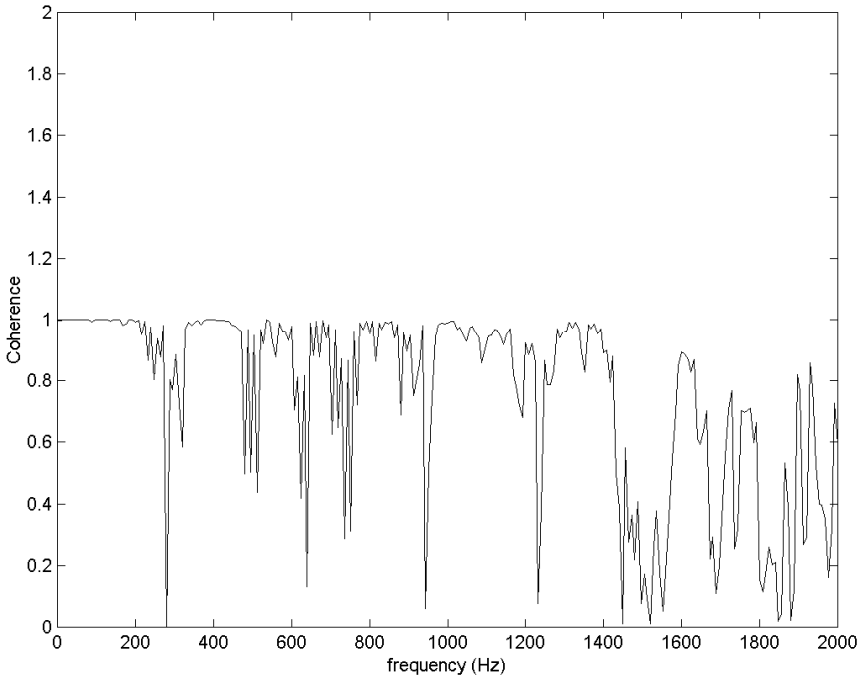

Figure: 4

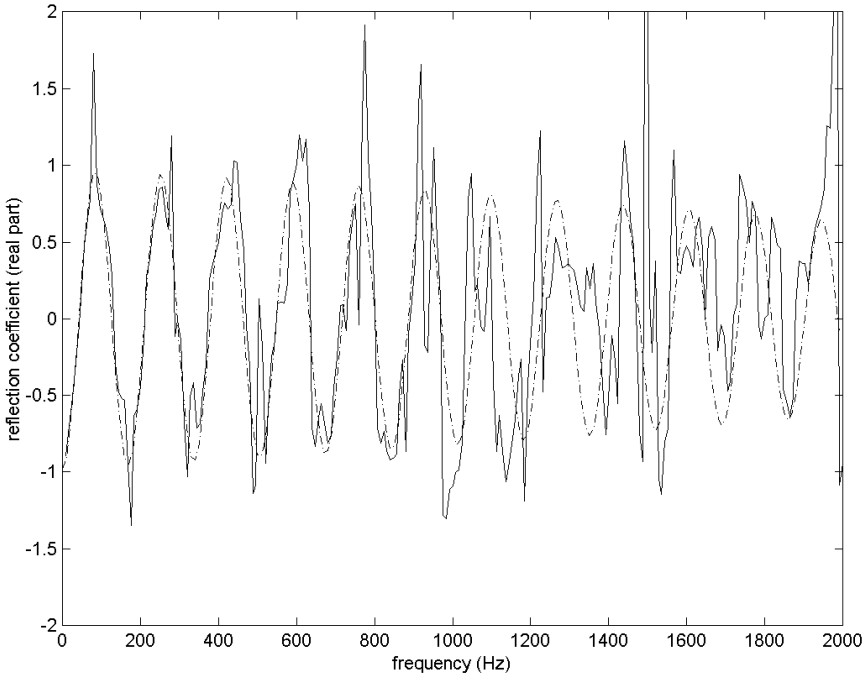

Figure: 5

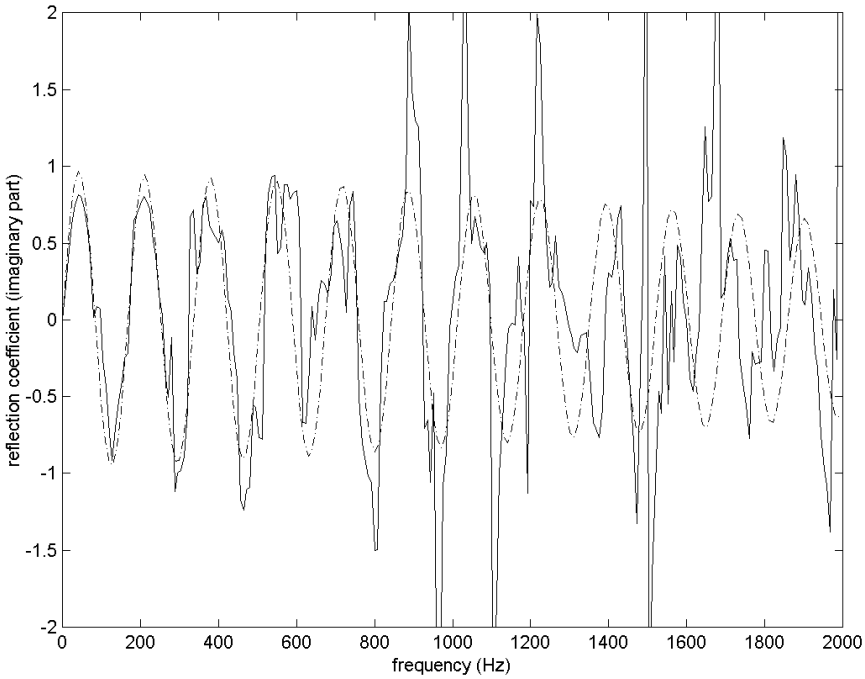

Figure: 6

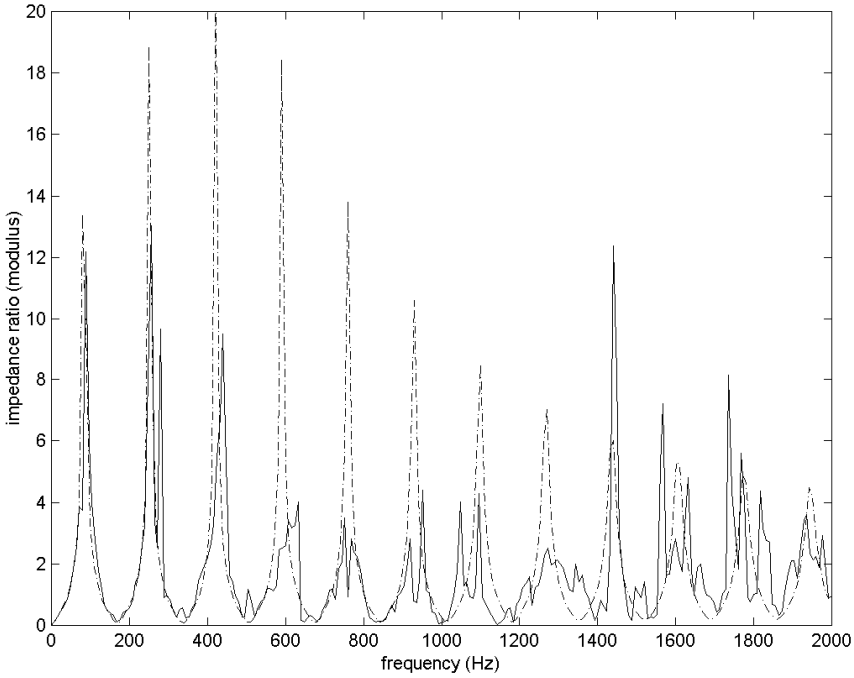

Figure: 7

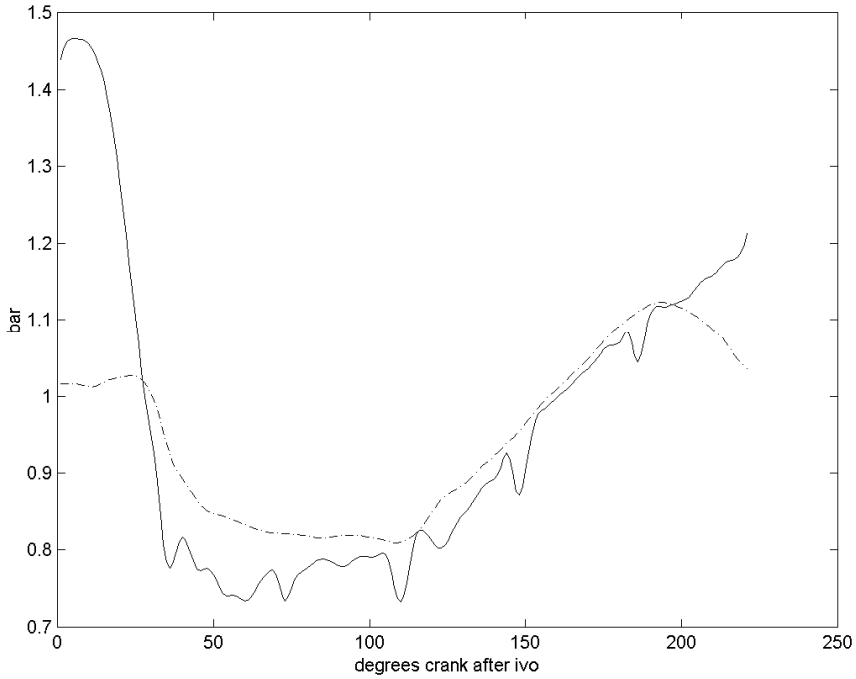

Figure: 8

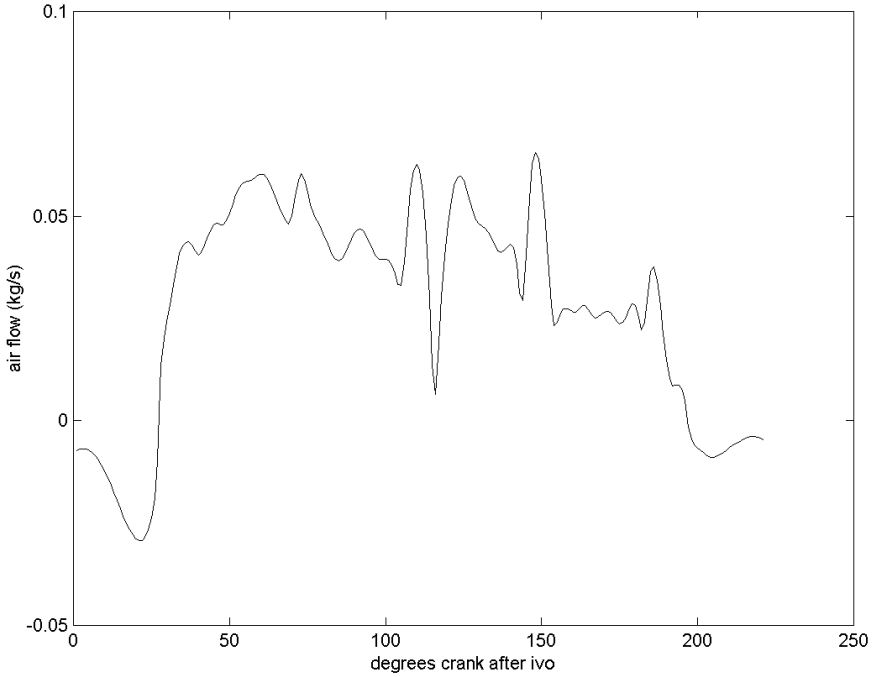

Figure: 9

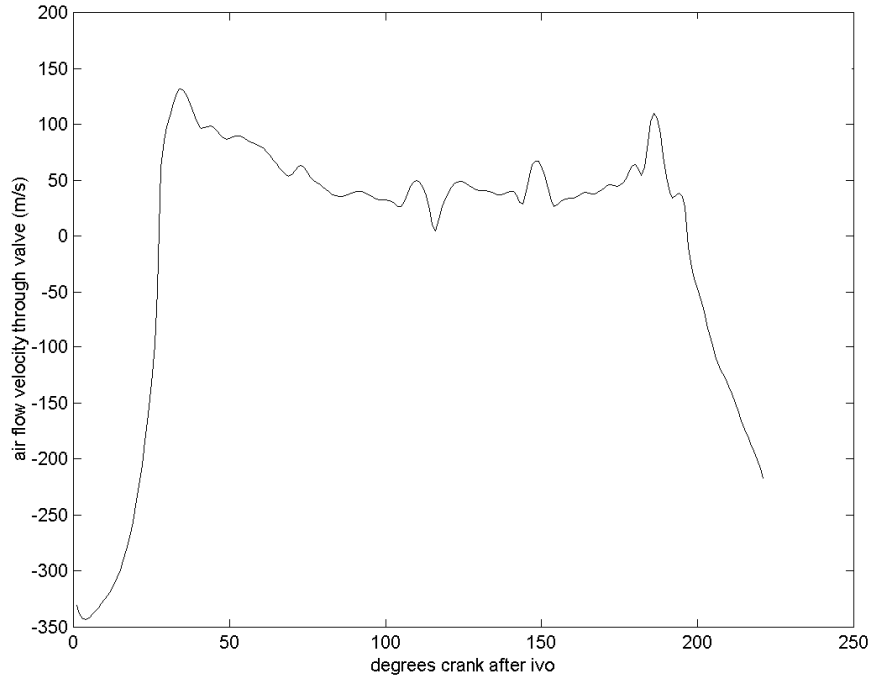

Figure: 10

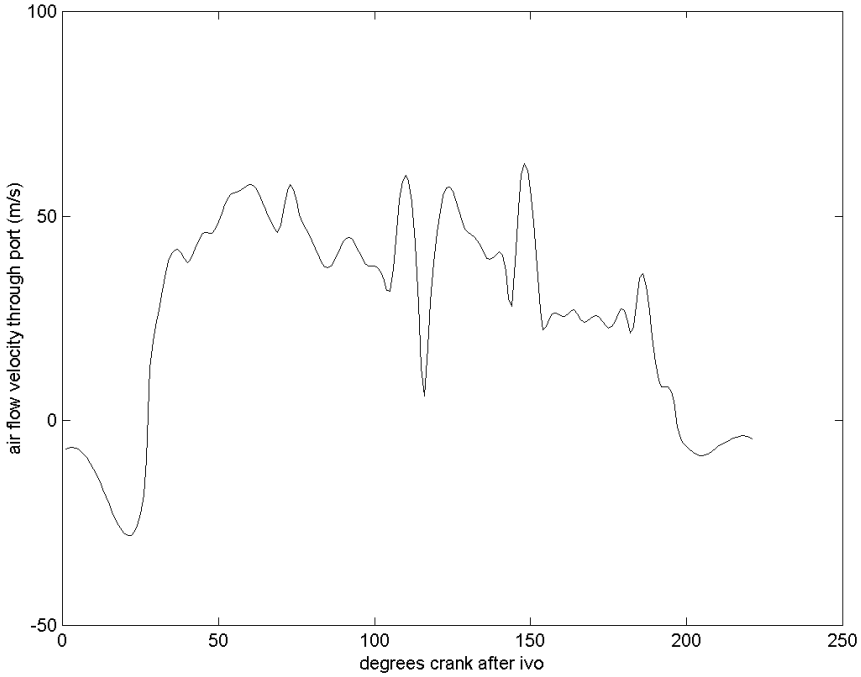

Figure: 11

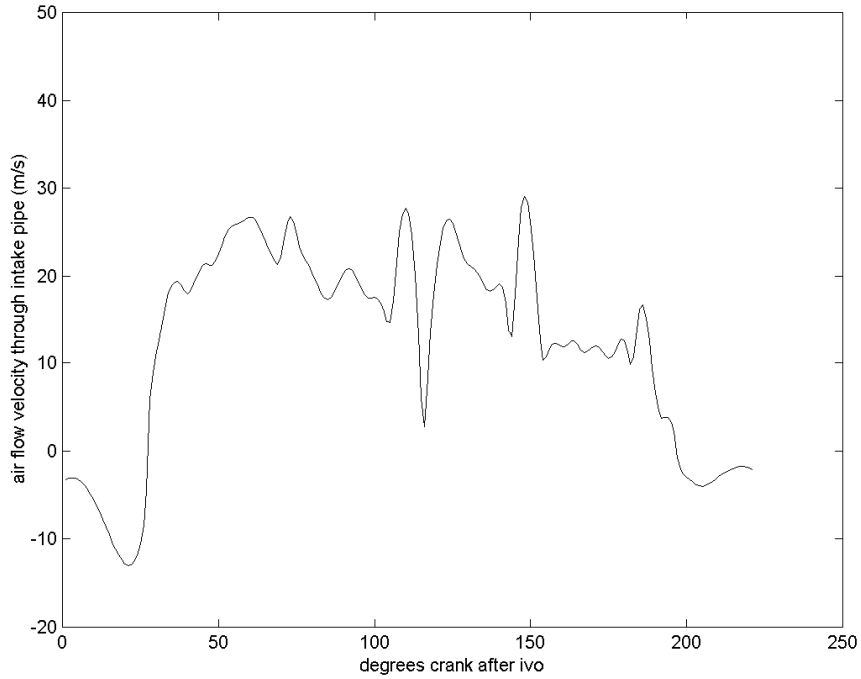

Figure: 12

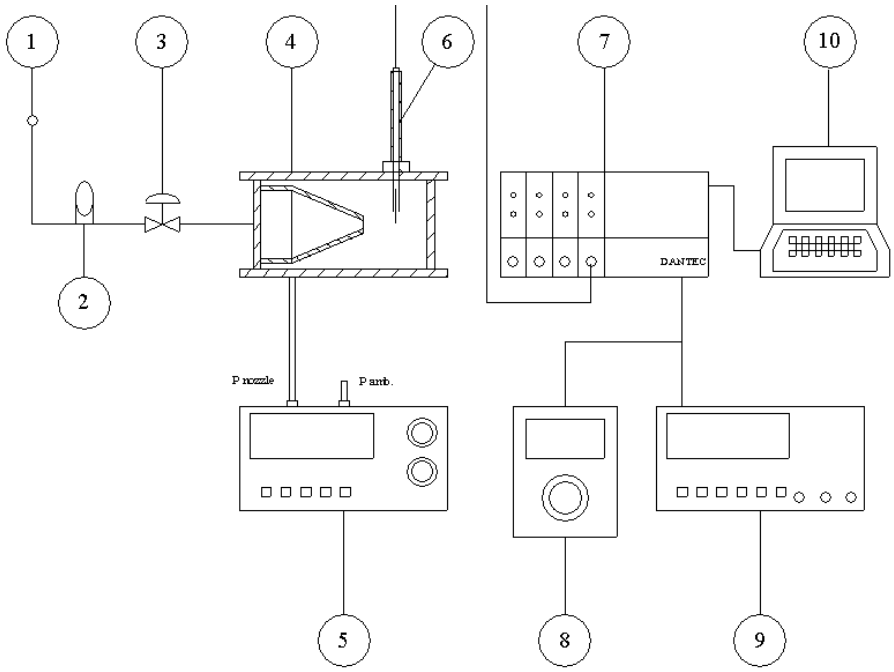

Figure: 13

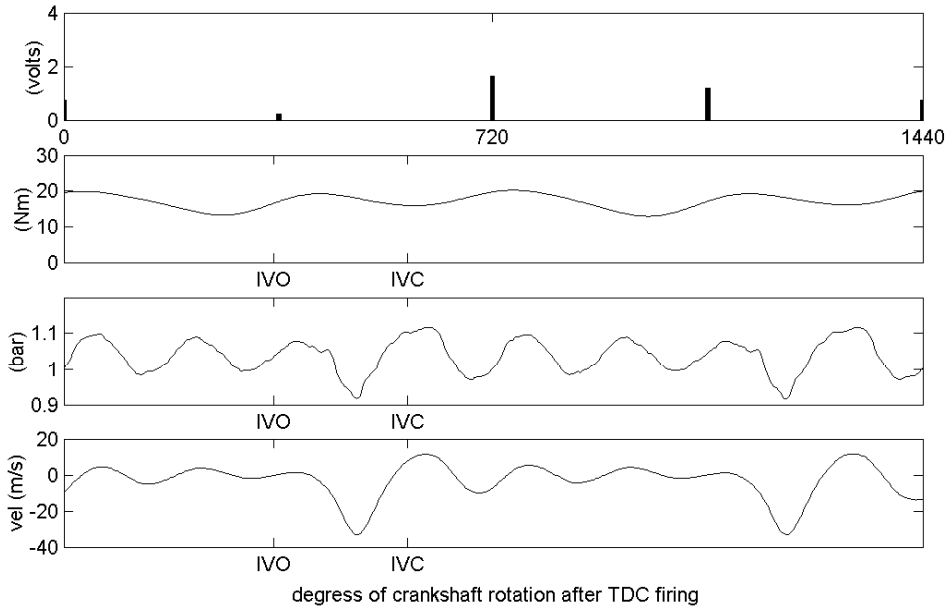

Figure: 14

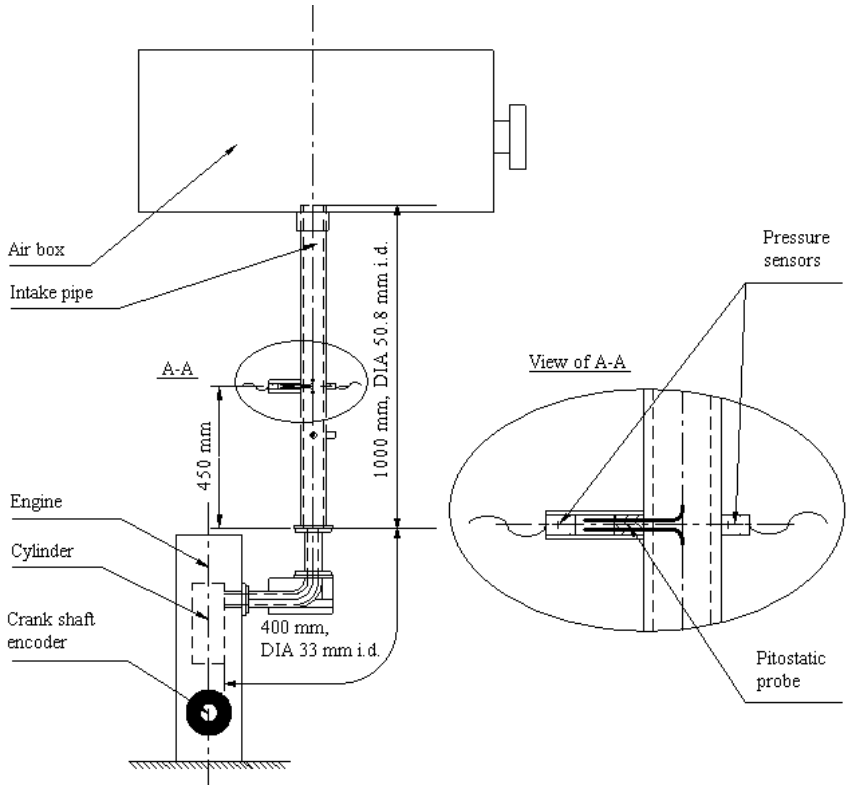

Figure: 15

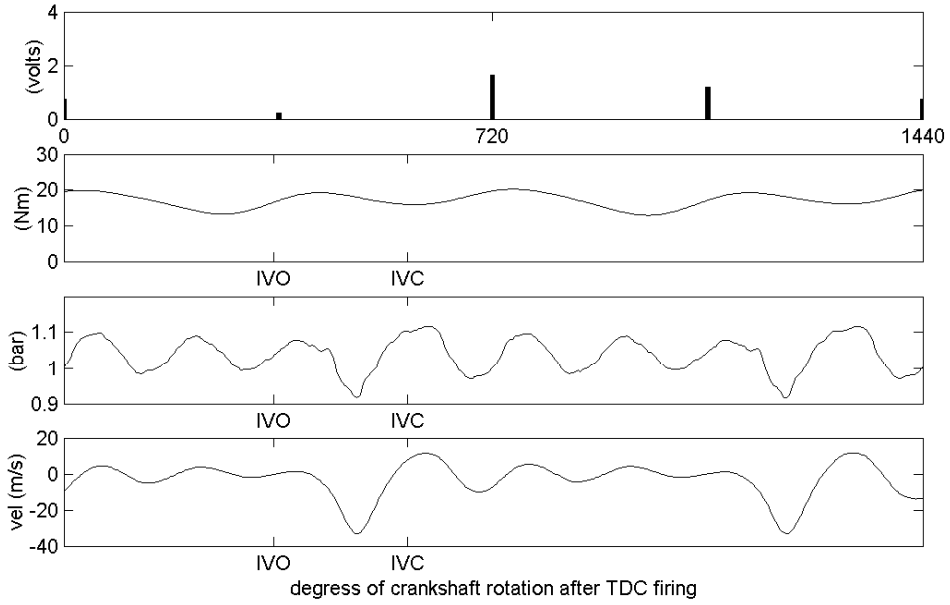

Figure: 16